Modeling the Transitional Kinematics Between Variable-Incline Walking and Stair Climbing

Shihao Cheng, Edgar Bolívar-Nieto, Cara Gonzalez Welker, and Robert D. Gregg

***Abstract*—Although emerging powered prostheses can enable people with lower-limb amputation to walk and climb stairs over different task conditions (e.g., speeds and inclines), the control architecture typically uses a finite-state machine to switch between activity-specific controllers. Because these controllers focus on steady-state locomotion, powered prostheses abruptly switch between controllers during gait transitions rather than continuously adjusting leg biomechanics in synchrony with the users. This paper introduces a new framework for powered prosthesis control by modeling the lower-limb joint kinematics over a continuum of variable-incline walking and stair climbing, including steady-state and transitional gaits. Steady-state models for walking and stair climbing represent joint kinematics as continuous functions of gait phase, forward speed, and incline. Transition models interpolate kinematics as convex combinations of the two steady-state models, with an additional term to account for kinematics that fall outside their convex hull. The coefficients of this convex combination denote the similarity of the transitional kinematics to each steady-state mode, providing insight into how able-bodied individuals continuously transition between ambulation modes. Cross-validation demonstrates that the model predictions of untrained kinematics have errors within the range of physiological variability for all joints. Simulation results demonstrate the model's robustness to incline estimation and mode classification errors.**

I. Introduction

Most commercially-available prostheses for above-knee amputees are mechanically passive or semi-active, so they cannot provide the net-positive work that is crucially important for inclined walking and stair climbing. Powered, or active, prostheses [1]–[3] can provide positive mechanical work to reduce the compensations and effort required for the user to walk [4]. In particular, powered prostheses attempt to mimic biological leg behavior (often using able-bodied kinematics as references [5]–[11]) to restore physiological gait biomechanics similar to an able-bodied population. The state-of-the-art control approach for multi-activity powered prostheses uses a finite state machine (FSM) to switch between different controllers for each ambulation mode [1], [12]–[15]. This control paradigm uses sensors such as inertial measurement units (IMUs) and/or electromyography signals to predict user intent in locomotion, including but not limited to level walking, ramp ascent/descent, and stair ascent/descent [16]. Therefore, at least five different controllers corresponding to each mode of locomotion are constructed separately, often with their own finite-state machines to represent gait progression [17]. This results in many control parameters that require domain knowledge to fully configure to each user [18]. Moreover, accurate and timely estimation of user intent has been a barrier in the field for years; classification errors can cause falls and reduce the user's confidence in the prosthetic leg [19].

In the past few years, researchers have attempted to combine FSM activity states by continuously parameterizing the joint kinematics with phase and task variables [7]–[10]. A phase variable refers to a biomechanical signal that measures the continuous gait progression during locomotion, such as thigh angle and its integral [5]. Task variables quantify continuous variations of an activity such as step length, gait speed, or ground incline. Based on this concept, Embry et al. [9], [10] modeled joint kinematics as a continuous function of gait phase, forward speed, and ground incline. This model successfully combined level walking and ramp walking under continuous variations in ground incline, which experimental implementations [20] have leveraged to continuously adapt to task conditions. Inspired by this continuously-varying walking model, we adopt this modeling framework and expand it to combine stair ascent and stair descent under continuous variations of stair inclination, in order to further reduce the number of separate ambulation modes.

The transitions between ambulation modes also remain an important challenge, as existing prosthesis controllers focus on steady-state gait. State-of-the-art control strategies discretely switch the prosthetic leg from one steady-state controller to another (e.g., walk to stair ascent) [13], [14] after the high-level controller estimates the intent of the user. However, switching in this manner can cause abrupt changes in control behavior, where certain timings within the gait cycle may result in gait instability [21] and fall risk for the users. Fortunately, emerging intent recognition algorithms are now making it possible to predict the transition before it happens using combinations of several IMUs [22] or a system consisting of a depth camera and IMU [23] with $> 93\%$ accuracy. This presents an opportunity for the controller to implement appropriate joint kinematics for a seamless and smooth transition between ambulation modes, as described in a recent study of the anticipatory kinematics of transitions from level walking to stair ascent and descent [24]. However, it is unclear how to model the continuously-varying kinematics during the transitions between stair ascent/descent and walk, let alone the relationships between steady-state and transitional

This work was supported by the National Institute of Child Health & Human Development of the NIH under Award R01HD094772. The content is solely the responsibility of the authors and does not necessarily represent the official views of the NIH. (Corresponding author: Robert D. Gregg)

S. Cheng is with the Department of Mechanical Engineering and the Robotics Institute, and C. Welker, E. Bolívar-Nieto and R. Gregg are with the Department of Electrical and Computer Engineering and the Robotics Institute, University of Michigan, Ann Arbor, MI, 48109 USA. Contact: chengsh@umich.edu; ebolivar@ieee.org; cara.welker@colorado.edu; rgregg@ieee.org

kinematics under different combinations of walking speed and ground/stair inclination.

To address these challenges, we present a modeling framework that represents the gait kinematics of steady-state walking and stair climbing as continuous functions of the phase, forward speed, and terrain inclination. We further model the transitional kinematics as a convex combination of these two steady-state kinematic models plus a conditional offset. By visualizing the coefficients of this convex combination and the conditional offset during transitions between walk and stairs, we establish a biomechanical relationship between transitional and steady-state kinematics at each phase. We train and validate our models with an open-source dataset [25]. Furthermore, we evaluate the robustness of the models against input perturbations and ambulation mode misclassification using Monte Carlo simulations. We consider this modeling framework an essential step towards a unified, non-switching, phase-based controller for powered prosthetic legs. The main contributions of the paper are summarized as follows:

- Extends the continuously-varying model [9] from variable-incline walking to variable-incline stair climbing, accounting for additional activities of daily life.
- Introduces a transition modeling framework to generate walk to stair and stair to walk models using a convex combination of the steady-state walk and stair models, which connects these steady-state activities within a continuous activity space.
- Introduces a conditional offset that applies at certain phases where the transition trajectories leave the convex hull of the two steady-state models, which offers insight into how transitions differ from the steady-state activities.
- Explores the biomechanical meaning behind the coefficients of the convex combination and the offset term in the transition models, which could guide future studies of locomotion mode transitions.
- Demonstrates the robustness of the continuously-varying models against perturbations in the inclination input and misclassification in ambulation mode during walking at low inclinations.

The rest of this paper is organized as follows. Section II introduces the formulation and evaluation methods of the modeling framework. Section III summarizes the results of model fitting and simulations. Section IV discusses these results and the future integration of the models with robotic prosthesis controllers, along with some limitations and future work. Finally, we conclude in Section V.

II. METHODS

In this section, we explain the modeling frameworks for the steady-state and transition models. We first describe the dataset used to train the models and the symbolic definition of modeling terms. Then, we introduce the constraints of the objective on the models and formulate the optimizations based on these constraints. Finally, we describe how we evaluate the accuracy and robustness of the models using cross-validation and offline simulations with the dataset. Supplementary Table S1 summarizes all the symbolic terms we use in this section.

A. Experimental Dataset

We used a publicly available dataset [25] of lower-limb kinematics and kinetics of ten able-bodied participants (five female, years: 30.4 $\pm$ 14.9, weight: 74.6 $\pm$ 9.7 kg, height: 1.73 $\pm$ 0.94 m) walking at multiple inclines ($\pm$ 0°, 5° and 10°) and speeds (0.8 $\mathrm{m\,s^{-1}}$, 1 $\mathrm{m\,s^{-1}}$ and 1.2 $\mathrm{m\,s^{-1}}$). It also contains stair data with multiple stair inclines ($\pm$ 20°, 25°, 30° and 35°), and the transitions between walk and stairs at those inclines. Data were collected using a Vicon motion capture system, and a Bertec instrumented treadmill was used to actuate different walking task conditions, i.e., different inclines and speeds. In this dataset, 0% gait cycle corresponds to heel strike, and this definition applies to the rest of the paper. The use of the data was approved by the Institutional Review Board at the University of Michigan under HUM00166976 on 08/13/2019.

B. Gait Model

We define the inputs to our models as the gait phase, forward speed, and ground/stair inclinations, and the output to be the joint angle for the hip, knee, or ankle. Based on this structure, we set up the following assumptions for our modeling framework. First, we assume that the gait cycle is periodic for the steady-state activities (i.e., steady-state walking and stair climbing). Second, we assume that the input variables to the models, e.g., forward speeds and ground/stair inclinations, are continuous. Third, we assume that the input speed and incline during daily locomotion are within the boundary values of our training dataset, which can easily be expanded in future work. Finally, we assume the average joint kinematics for the steady-state modes before and after a transition are known. The practical implications of these assumptions are discussed in Section IV.

We first introduce the steady-state walking (SSW) model proposed by Embry et al. [9] and the extension to the steady-state stair (SSS) model. Then, we detail the modeling of the transitional models, i.e., walk to stair (W2S) and stair to walk (S2W), based on the two steady states. For the steady-state models, we represent joint kinematics as a function of gait phase (ϕ) and task condition (χ), where the gait phase refers to the phase variable. The task condition contains two dimensions, $\chi = (v, \iota)$, where v and ι are the subject's forward speed and the ground/stair inclination, respectively. Since the speed was self-selected in the steady and transitional stair kinematics in the training dataset [25], we assume a nominal forward speed (1 $\mathrm{m\,s^{-1}}$) during SSS, W2S, and S2W model training. Similarly, the W2S and S2W models are generated for level walking based on the available data. These dimensions could be expanded once additional training data becomes available. The stair incline in the dataset [25] was defined as $\iota = \mathrm{atan}(\frac{h_s}{d_s})$, where h_s and d_s represent the total height and length of the staircase used to collect the data, respectively. We map the range of stair inclines (from $-35°$ to 35°) to a normalized range of 0 to 1, which helps to parameterize the task function and generalize the modeling framework to different datasets. We consider level walking as a 0° stairs condition in order to connect stair ascent and descent, despite missing data for absolute stair inclines less than 20°.

As in Embry et al. [9], the steady-state kinematics are modeled as a weighted sum of N basis functions of gait phase, $b_k(\phi)$, and the weight of each basis function is described by the task function $c_k(\chi)$. The basis functions $b_k(\phi)$ are finite Fourier series of degree $F = 10$, and the task functions are parameterized as Bernstein basis polynomials [9]. Therefore, we express the joint angle θ of the hip, knee, and ankle as

$$\theta(\phi,\chi) = \sum_{k=1}^{N} b_k(\phi)c_k(\chi), \tag{1}$$

$$b_k(\phi) = \beta_{00k} + \sum_{i=1}^{F} \left(\beta_{1ik}\cos(i\phi) + \beta_{2ik}\sin(i\phi)\right), \tag{2}$$

$$c_k(\chi) = \begin{pmatrix} \lambda \\ \kappa \end{pmatrix} f(\chi)^{\kappa}(1-f(\chi))^{\lambda-\kappa}, \tag{3}$$

where the basis functions are indexed by $k = 1,\ldots,N$ in (1), $\beta_{tik} \in R$ in (2) are the Fourier coefficients to optimize, and λ, κ are the binomial coefficients described next.

We chose the order of Bernstein polynomial in order to capture the complexity of the input dimension without over-fitting. The order of Bernstein polynomial is given by λ, and κ is the set of integers that goes from 0 to λ to form the Bernstein basis. For example, if $\lambda = 3$, the Bernstein basis contains four terms as $\kappa = \{0,1,2,3\}$ (details in [9]). Although we were unable to train the SSS on different speeds, we used second-order Bernstein basis polynomials to model the speed dimension as in the SSW walking model. However, due to the increasing complexity of kinematic changes between stair ascent, level walking, and stair descent across inclines, we chose $4^{th}, 7^{th}$, and 6^{th} order of Bernstein basis polynomial for the hip, knee, and ankle, respectively. For SSW, 3^{rd} order is enough to describe the kinematic changes with inclines [9].

To formulate a convex optimization program, we define the optimization variable x as

$$x_k = [\beta_{00k}\ \beta_{11k}\ \beta_{21k}\ \ldots\ \beta_{1Fk}\ \beta_{2Fk}]^T \in \mathbb{R}^{1+2F},$$
$$x = [x_1\ x_2\ \ldots\ x_N] \in \mathbb{R}^{(1+2F)\times N}.$$

A matrix L stores the phase dependent terms in (2):

$$\ell_i = [1\ \cos(\phi_i)\ \sin(\phi_i)\ \ldots\ \cos(F\phi_i)\ \sin(F\phi_i)] \in \mathbb{R}^{1\times(1+2F)},$$
$$L = [\ell_1\ \ell_2\ \ldots\ \ell_P]^T \in \mathbb{R}^{P\times(1+2F)},$$

where P is the number of discrete gait phases indexed by i. A matrix U stores the terms of N task functions in (3):

$$u_j = [c_1(\chi_j)\ c_2(\chi_j)\ \ldots\ c_N(\chi_j)]^T \in \mathbb{R}^{N\times 1},$$
$$U = [u_1\ u_2\ \ldots\ u_G] \in \mathbb{R}^{N\times G},$$

where G is the number of discrete task conditions indexed by j. G is equal to 15 for the walking model and 9 for the stair and transition models based on the available dataset [25].

The model in (1) fits the experimental data by optimal design of the parameters x. For each gait phase (ϕ_i) and task (χ_j), the model is linear with respect to the parameters and the joint angle can be expressed as

$$\ell_i x u_j = \sum_{k=1}^{N} b_k(\phi_i)c_k(\chi_j). \tag{4}$$

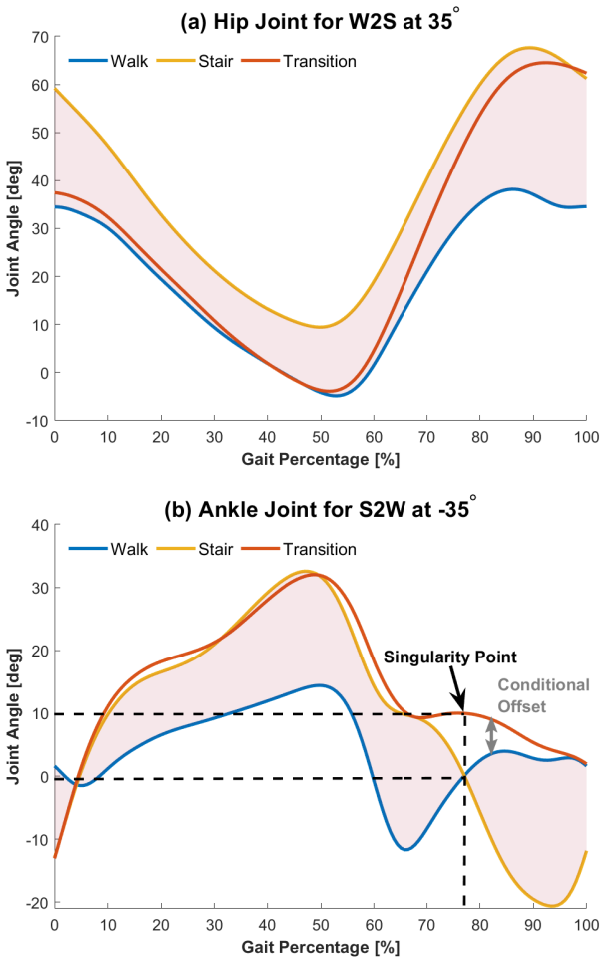

Fig. 1. (a) Ideal case: For W2S, transitional kinematics are close to walking kinematics at the beginning but tend to stair kinematics towards the end of the gait cycle. This plot demonstrates that the transition trajectory is within the convex hull created by the walking and stair trajectories (red shaded area). (b) Non-ideal case: The transition trajectory is outside the convex hull region to show the necessity of the conditional offset term (e.g., the gray double arrow). The singularity point on the plot occurs when the walk and stair trajectories intercept at $\approx 0°$ while the transition trajectory is higher than both trajectories, which would create discontinuities without the conditional offset term.

To generate the transition models as functions of the steady-state models, we model the S2W and W2S transitional kinematics using a convex combination of SSW and SSS kinematics with a conditional offset (Fig. 1(a)):

$$\begin{aligned}\theta^{ts}(\phi,\chi) =& \alpha(\phi,\chi)\theta^{w}(\phi,\chi^{w}) \\ &+ (1-\alpha(\phi,\chi))\theta^{s}(\phi,\chi^{s}) + O(\phi,\chi)\gamma(\phi,\chi),\end{aligned} \tag{5}$$

$$O(\phi,\chi) = \begin{cases} 1 & \theta^{ts}(\phi,\chi) > \max(\theta^{w}(\phi,\chi^{w}),\theta^{s}(\phi,\chi^{s})), \\ 1 & \theta^{ts}(\phi,\chi) < \min(\theta^{w}(\phi,\chi^{w}),\theta^{s}(\phi,\chi^{s})), \\ 0 & \text{otherwise}, \end{cases} \tag{6}$$

$$\alpha(\phi,\chi) = \sum_{k=1}^{M} a_k(\phi)c_k(\chi), \tag{7}$$

$$\gamma(\phi,\chi) = \sum_{k=1}^{M} r_k(\phi)c_k(\chi), \tag{8}$$

where θ^{ts}, θ^{w}, θ^{s} are the joint angles of the W2S/S2W, SSW, and SSS models, respectively. O is the indicator function that determines whether the transition joint angle is outside the convex hull created by steady-state walk and stair models at each point in time. We introduced the conditional offset term $O(\phi,\chi)\gamma(\phi,\chi)$ based on the observation that the transition trajectories are not always in between the corresponding walk and stair trajectories (e.g., Fig. 1(b)). Because the dataset had only a discrete set of inclines, we linearly interpolated the conditional offset term when generating the final transition models across a continuum of inclinations. χ^{w},χ^{s} represent the measured task condition inputs to the SSW and SSS models, respectively, before or after the transition. α is the non-negative convex coefficient and γ is the offset angle, which are both weighted summations of M functions of gait phase and task conditions. $c_k(\chi)$ here is a 2^{nd}-order Bernstein basis polynomial, while $a_k(\phi)$ and $r_k(\phi)$ are undefined phase functions that need to be solved with the convex optimization.

To formulate a convex optimization program, we define a matrix V to store M task functions in (7) and (8):

$$v_j = [c_1(\chi_j)\ c_2(\chi_j)\ \dots\ c_M(\chi_j)]^T \in \mathbb{R}^{M\times 1},$$
$$V = [v_1\ v_2\ \dots\ v_G] \in \mathbb{R}^{M\times G}.$$

Similar to (4), at each gait phase (ϕ_i) and task condition (χ_j), the coefficients α and γ can be expressed as

$$y_i v_j = \sum_{k=1}^{M} a_k(\phi_i)c_k(\chi_j), \tag{9}$$

$$z_i v_j = \sum_{k=1}^{M} r_k(\phi_i)c_k(\chi_j), \tag{10}$$

where $y_i \in \mathbb{R}^{1\times M}$ and $z_i \in \mathbb{R}^{1\times M}$ are the i^{th} row of the optimization variables $y \in \mathbb{R}^{P\times M}$ and $z \in \mathbb{R}^{P\times M}$, respectively.

Substituting (9) and (10) into (5), we can write

$$\Theta^{ts}_{ij} = \theta^{ts}(\phi_i,\chi_j) = \begin{bmatrix} y_i & z_i \end{bmatrix} \begin{bmatrix} v_j(w-s) \\ v_j o \end{bmatrix} + s, \tag{11}$$

where $w = \theta^{w}(\phi_i,\chi^{w}_j)$ and $s = \theta^{s}(\phi_i,\chi^{s}_j)$ are the known joint angles from SSW, SSS at given task condition and phase, $o = O(\phi_i,\chi_j)$ is either 0 or 1 depending on whether the transition joint angle is outside the convex hull region, Θ^{ts}_{ij} is the i^{th} row and j^{th} column of the transitional joint kinematics matrix $\Theta^{ts} \in \mathbb{R}^{P\times G}$. Therefore, the transitional joint kinematics are affine functions of the optimization variables y and z. Note that we fix $\chi_w = (1\,\mathrm{m\,s^{-1}}, 0^\circ)$ for the later analysis on the transition models.

C. Model Training

We formulate a convex optimization problem to train all the models, ensuring that each optimum is a global optimum. As a prerequisite, we set up the objective and all constraints to be convex functions [26]. We then solve the optimization variable x for the steady-state models (SSW and SSS), and the optimization variables y and z for the transition models (W2S and S2W). The variables x, y, and z store the coefficients of the task and/or basis functions, as discussed in Section II-B. This subsection focuses on the model training process for the transition models; we will only briefly introduce the steady-state models as the detailed modeling is available in [9].

1) Fitting to Averaged Kinematics: All the steady-state and transition training share the same main optimization objective: fitting the models to the average able-bodied kinematics for a range of task conditions. Because the variance in the experimental kinematics is non-constant over phase, we divide the difference between the model output and the average joint angle by the standard deviation at each phase and task condition to weight measurements according to uncertainty. To that end, we define the first minimization objective as

$$\left\| (\bar{\mathbf{d}}_{\phi\chi} - LxU) \oslash SD(\mathbf{d}_{\phi\chi}) \right\|_2, \tag{12}$$

where $\oslash$ is the element-wise matrix division known as Hadamard Division [27], $\bar{\mathbf{d}}_{\phi\chi} \in \mathbb{R}^{P\times G}$ is the inter-subject mean of joint kinematics, $SD(\mathbf{d}_{\phi\chi}) \in \mathbb{R}^{P\times G}$ is the standard deviation, and $LxU \in \mathbb{R}^{P\times G}$ is the model's predicted joint kinematics across all phases (ϕ_i) in the row and task conditions (χ_j) in the column with each element calculated by (4).

2) Jerk Minimization: Jerk minimization is important to guarantee the smoothness of the model outputs and ensure the predicted trajectories can reflect natural human motions [9], [28]. Because the jerk can be calculated by the third derivative of the actual trajectories, and we train the model based on discretized phases and task conditions, we define a discrete unitless derivative operator D as a matrix:

$$D = \begin{bmatrix} -1 & 1 & 0 & \dots & 0 \\ 0 & -1 & 1 & 0 & \vdots \\ 0 & 0 & \ddots & \ddots & 0 \\ \vdots & \vdots & 0 & -1 & 1 \\ 0 & 0 & 0 & 0 & 0 \end{bmatrix} \in \mathbb{R}^{P\times P}.$$

By multiplying the D matrix three times with the joint kinematics matrix $LxU \in \mathbb{R}^{P\times G}$, we can minimize the discrete jerk for the steady-state models as our second objective:

$$\|SLxU\|_2, \tag{13}$$

where $S = DDD \in \mathbb{R}^{P\times P}$.

In addition to the joint jerk minimization in the steady-state models, we also want to minimize the jerk of the α and γ terms for the transition models. Since the convex optimization tends to find the solution that fits the training data best by sacrificing the smoothness of α, we minimize its jerk to avoid abrupt changes over phase. Otherwise, biomechanically infeasible motion such as instantaneous ambulation mode transition may arise. Minimizing the jerk of γ helps to further smooth the model outputs when the conditional offset applies. Therefore, we write the last minimization objective as

$$\|SyV\|_1 + \|SzV\|_1, \tag{14}$$

In this case we use the L_1 norm, as it is more robust against outliers in order to keep the overall jerk of the interpolation coefficients small.

3) Optimization Constraints: For the steady-state models, we set up box constraints on the range of motion ($[R_{min}, R_{max}]$) for each joint by constraining the magnitude of each task function before we solve for x [9]. For the transition models, we apply alternative constraints on α and γ to ensure uniqueness and biomechanical meaning of the solution. Those constraints can also guarantee the range of motion is well-bounded since we model transition kinematics as a convex combination of walk and stair and the jerk of γ is minimized. First, since we set up the transitional kinematics as the convex combination of the walk and stair kinematics with conditional offsets, based on Jensen's inequality [26], we introduce $0 \leq \alpha \leq 1$. In this way, we constrain the transition trajectories to be inside the convex hull created by the walking and stair trajectories. Second, we intuit that the transition trajectories should start at the state from which they are transitioning and converge to the state to which they are transitioning. Based on this, we constrain α to be close to 1 at the beginning of the walk to stair transition and α to be close to 0 at the beginning of the stair to walk transition. Third, we constrain α to be strictly monotonically increasing during S2W or strictly monotonically decreasing during W2S to model unidirectional transitions.

4) Convex Optimization Formulation: Given the objectives and constraints in Section II-C up to this point, we formulate the convex optimization programs to find the optimal model parameters for the steady-state and transition models separately. For the steady-state models, we have

$$\begin{aligned} \min_{x,\rho} \quad & \rho + \delta \left\| SLxU \right\|_2, \\ \text{s.t.} \quad & -\rho \,\mathrm{SD}\left(\mathbf{d}_{\phi_i \chi_j}\right) \leq \overline{\mathbf{d}}_{\phi_i x_j} - \ell_i x u_j \leq \rho \,\mathrm{SD}\left(\mathbf{d}_{\phi_i \chi_j}\right), \\ & R_{min} < R_i^{\min}, \\ & R_{max} > R_i^{\max}, \\ & i = 1,2,\ldots,P \text{ and } j = 1,2,...,G, \end{aligned} \tag{15}$$

where ρ characterizes the accuracy of data fitting, and δ is the weight on jerk minimization. Following [9], $\delta = 10^{-5}$ was selected for the steady-state models. $R_i^{\max}, R_i^{\min}$ are the maximum and minimum joint positions, respectively, at discrete phase ϕ_i.

The transition models are similar to the optimization program (15), but with additional jerk minimization and constraints on the α and γ coefficients. For example, the W2S model training is set up as follows:

$$\begin{aligned} \min_{y,z,\sigma,\rho} \quad & \sigma + \rho + \delta \left\| S\Theta^{ts} \right\|_2 + \varepsilon \left\| SyV \right\|_1 + \eta \left\| SzV \right\|_1, \\ \text{s.t.} \quad & -\rho \,\mathrm{SD}\left(\mathbf{d}_{\phi_i \chi_j}\right) \leq \overline{\mathbf{d}}_{\phi_i x_j} - \Theta_{ij}^{ts} \leq \rho \,\mathrm{SD}\left(\mathbf{d}_{\phi_i \chi_j}\right), \\ & 0 \leq y_i v_j \leq 1, \\ & \left\| y_1 v_j - 1 \right\|_2 \leq \sigma, \\ & DyV < 0, \\ & i = 1,2,\ldots,P \text{ and } j = 1,2,...,G, \end{aligned} \tag{16}$$

where δ, ε, and η are the weighting coefficients for the jerk minimization of the joint and interpolation coefficients. DyV gives the discrete first-order derivative of the α coefficient to constrain the monotonicity.

For the S2W modeling, the optimization program is the same as (16) except the constraints on the initial condition of α are close to 0 instead of 1, and α is monotonically increasing instead of decreasing.

For both transition models, we tuned the weighting coefficients based on the smoothness of the model output and the priority of each jerk minimization term, resulting in $\delta = 10^{-2}$, $\varepsilon = 1$, and $\eta = 7 \times 10^{-5}$. The optimization programs (15) and (16) reach a global minimum because they are convex optimization programs [26]. For the program (15), $\overline{\mathbf{d}}_{\phi_i x_j} - \ell_i x u_j$ is affine with respect to the optimization variable x, so the upper bound $\rho \,\mathrm{SD}\left(\mathbf{d}_{\phi_i \chi_j}\right)$ and lower bound $-\rho \,\mathrm{SD}\left(\mathbf{d}_{\phi_i \chi_j}\right)$ form affine constraints [9]. For the jerk minimization term, $\ell_i x u_j$ is linear with respect to vector x, and the L_2 norm of linear expression $SLxU$ is convex. The positive sum of this convex function and the affine expression ρ yields a convex objective. The convexity analysis for the program (16) follows the same logic as (15).

D. Model Evaluation

Each model is trained and evaluated using MATLAB R2019a (MathWorks, USA) on an Intel(R) Core(TM) i7-8700 CPU @ 3.00GHz, 8-Core processor (Intel Corporation, USA). We perform leave-one-out cross-validation to evaluate the models in terms of accuracy and robustness over inclines. Since no speed information is available for stairs and associated transitions in the dataset, model performance at different speeds for the SSS, W2S, and S2W models cannot be evaluated. Thus, we fix the speed input to those models and focus the analysis on the incline dimension.

1) Cross-Validation: To evaluate the predictive performance and generalizability of each model, we perform a leave-one-out cross-validation by removing one incline condition from the training data for use as testing data, and repeat this process for different inclinations. Let $H_w = \pm\{0,5,10\}^\circ$ and $H_s = \pm\{0,20,25,30,35\}^\circ$ denote the ground (i.e., walk) and stair inclinations in the dataset. Since we assumed the incline input to the model is always within the boundary, we focus the analysis on interpolation of the joint kinematics for (left out) walking inclines strictly between $\pm 10^\circ$ and stair inclines strictly between $\pm 35^\circ$. We do not leave out 0° in the stair model, which corresponds to the level walking trajectory, because its primary purpose was to connect the positive and negative inclines in order to help the model fitting.

Take the W2S model for example: in the first iteration, we separate H_s into the training set $H_s^T = \{-35,-25,-20,0,20,25,30,35\}^\circ$ and validation set $H_s^V = \{-30\}^\circ$. Then, H_s^T is used to fit the W2S model, and the kinematics data at H_s^V is used for comparison with the model output at the same inclination. In this way, we obtain the model performance under interpolation. For the SSW model, we repeat the validation step for each fixed speed.

2) Model Accuracy and Efficiency: For each iteration in the cross-validation, we quantify the model accuracy by the difference between the predicted kinematics $\theta(\phi_i, \chi_j)$ with the reference average kinematics $\overline{\mathbf{d}}_{\varphi_i x_j}$ using the validation set. First, the root-mean-square error (RMSE) is calculated down to the nearest hundredth of a degree, which is within the resolution of the joint angle estimates from the Plug In Gait model from Vicon [29]. Next, to account for the inter-subject variation, we normalize the absolute difference by the standard

TABLE I
SUMMARY STATISTICS OF MEANS, MAXIMUMS, AND RMSE OF CROSS-VALIDATION*

	Hip			Knee			Ankle		
	N_μ	N_m	RMSE (°)	N_μ	N_m	RMSE (°)	N_μ	N_m	RMSE (°)
SSS	0.15(0.09)	0.36(0.12)	1.64(0.89)	0.22(0.14)	0.71(0.29)	1.72(0.93)	0.16(0.07)	0.46(0.17)	1.34(0.63)
SSW	0.24(0.04)	0.57(0.14)	2.39(0.57)	0.45(0.24)	1.16(0.56)	2.99(1.19)	0.47(0.10)	1.13(0.29)	2.16(0.44)
W2S	0.21(0.10)	0.51(0.23)	2.21(0.89)	0.32(0.17)	0.98(0.70)	3.59(2.27)	0.29(0.10)	0.88(0.26)	1.80(0.61)
S2W	0.13(0.05)	0.34(0.11)	1.40(0.43)	0.28(0.07)	0.70(0.15)	2.67(0.90)	0.31(0.11)	0.87(0.42)	1.77(0.66)

* Table entries are in the form of mean (standard deviation) of the cross-validation for each evaluation metric and each joint. N_μ is the mean and N_m is the maximum of the normalized error, as defined in (17) and (18), respectively.

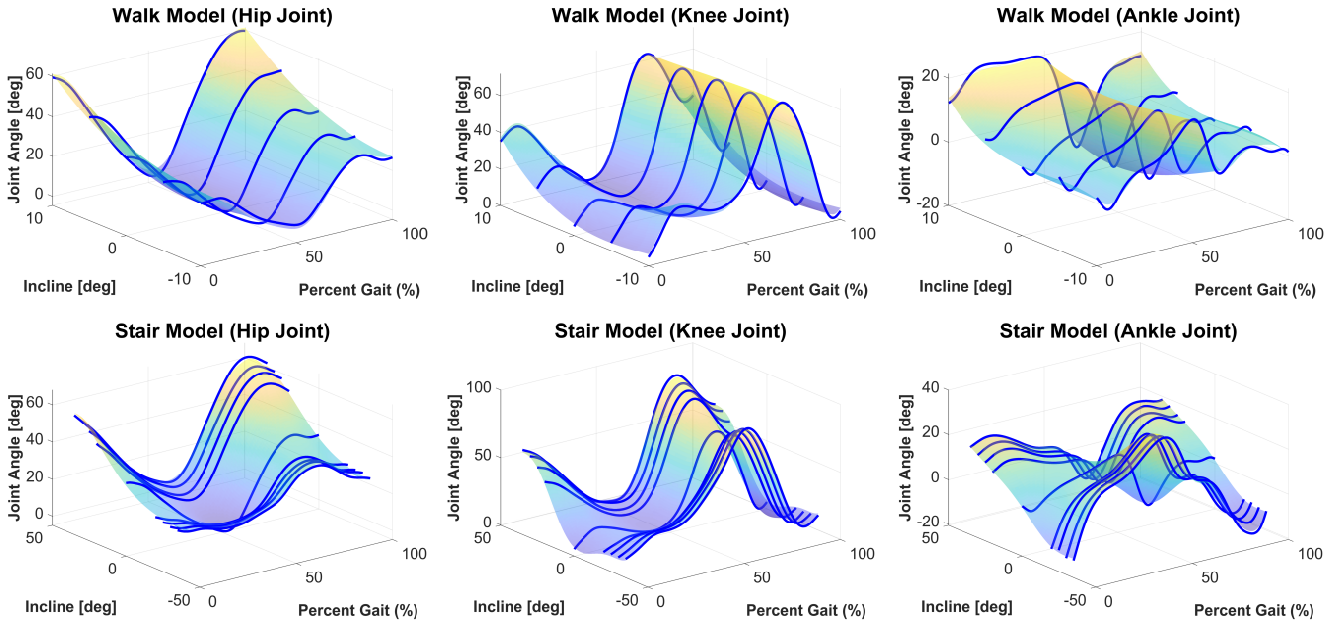

Fig. 2. Final continuously-varying walk (top) and stair (bottom) models for the hip, knee, and ankle joint generated using all the training data (blue lines). The four-dimensional walk model is projected onto one speed ($1.0\,\mathrm{m\,s^{-1}}$) in the top figure. The stair model assumes a single nominal speed ($1.0\,\mathrm{m\,s^{-1}}$), but it can easily be expanded when training data with different speeds become available. Note that level walking data was included in the stair model to connect stair ascent and stair descent and enable extrapolation of stair trajectories at lower inclinations (i.e., less than 20°).

deviation of the reference kinematics across all subjects at each phase and find the mean and maximum of the normalized error over phase. We denote the normalized mean error as N_μ and the normalized max error as N_m. Specifically, for each iteration, these errors are calculated as

$$N_\mu^c = \underset{i}{\text{mean}} \left| \frac{\bar{\mathrm{d}}_{\phi_i \chi_j} - \theta(\phi_i, \chi_j)}{\mathrm{SD}\left(\mathbf{d}_{\phi_i x_j}\right)} \right|, \quad i = 1,2,\ldots,P, j \in I^V, \text{ and } c = 1,2,\ldots r, \tag{17}$$

$$N_m^c = \underset{i}{\max} \left| \frac{\bar{\mathrm{d}}_{\phi_i \chi_j} - \theta(\phi_i, \chi_j)}{\mathrm{SD}\left(\mathbf{d}_{\phi_i x_j}\right)} \right|, \quad i = 1,2,\ldots,P, j \in I^V, \text{ and } c = 1,2,\ldots r, \tag{18}$$

where c refers to the iteration number and r is the total number of iterations for the cross-validation.

Model efficiency is evaluated by examining the model training time (time to generate an individual model from training data) and the model computation time (time for a trained model to output the joint angles given model inputs).

3) Robustness Analysis: We evaluate the robustness of the models from two perspectives: 1) robustness under perturbed model input, and 2) robustness under misclassification in ambulation modes. This first evaluation considers inevitable errors in the incline estimate. To that end, we perform a Monte Carlo simulation analysis at each incline in the dataset, where incline estimates are randomly sampled from a uniform distribution with a maximum error range of ±3.0° for SSS and transition models and ±1.5° for SSW. We select this error range based on the reported errors in previous systems for ramp incline estimation [20], [30] and for stair height estimation [31]. We convert the stair height to stair inclination based on the relationship reported in the supplementary documents of [25], which contains the recorded stair height corresponding to each stair inclination. Then, we repeat the Monte Carlo simulation with an increasing number of samples until convergence of the mean RMSE (normalized by joint ROM). Finally, the worst-case scenario with the maximum normalized RMSE among all the iterations is analyzed.

Our previous work in activity recognition [32] suggests that activity mode misclassifications most frequently occur

TABLE II
SUMMARY STATISTICS OF MEANS, MAXIMUMS, AND RMSE OF FINAL MODEL*

	Hip			Knee			Ankle		
	N_μ	N_m	RMSE (°)	N_μ	N_m	RMSE (°)	N_μ	N_m	RMSE (°)
SSS	0.11(0.04)	0.23(0.01)	1.12(0.30)	0.15(0.06)	0.34(0.01)	1.17(0.41)	0.08(0.02)	0.15(0.01)	0.63(0.20)
SSW	0.18(0.031)	0.32(0.10)	1.74(0.37)	0.35(0.10)	0.75(0.19)	2.21(0.29)	0.21(0.02)	0.43(0.04)	0.94(0.06)
W2S	0.19(0.07)	0.42(0.10)	2.11(0.69)	0.30(0.14)	0.68(0.18)	3.05(1.47)	0.27(0.09)	0.62(0.18)	1.72(0.60)
S2W	0.12(0.03)	0.26(0.03)	1.30(0.26)	0.30(0.08)	0.66(0.17)	2.78(0.92)	0.28(0.09)	0.77(0.35)	1.59(0.52)

*Table entries are in the form of mean (standard deviation) for each evaluation metric and each joint. N_μ is the mean and N_m is the maximum of the normalized error, as defined in (17) and (18), respectively.

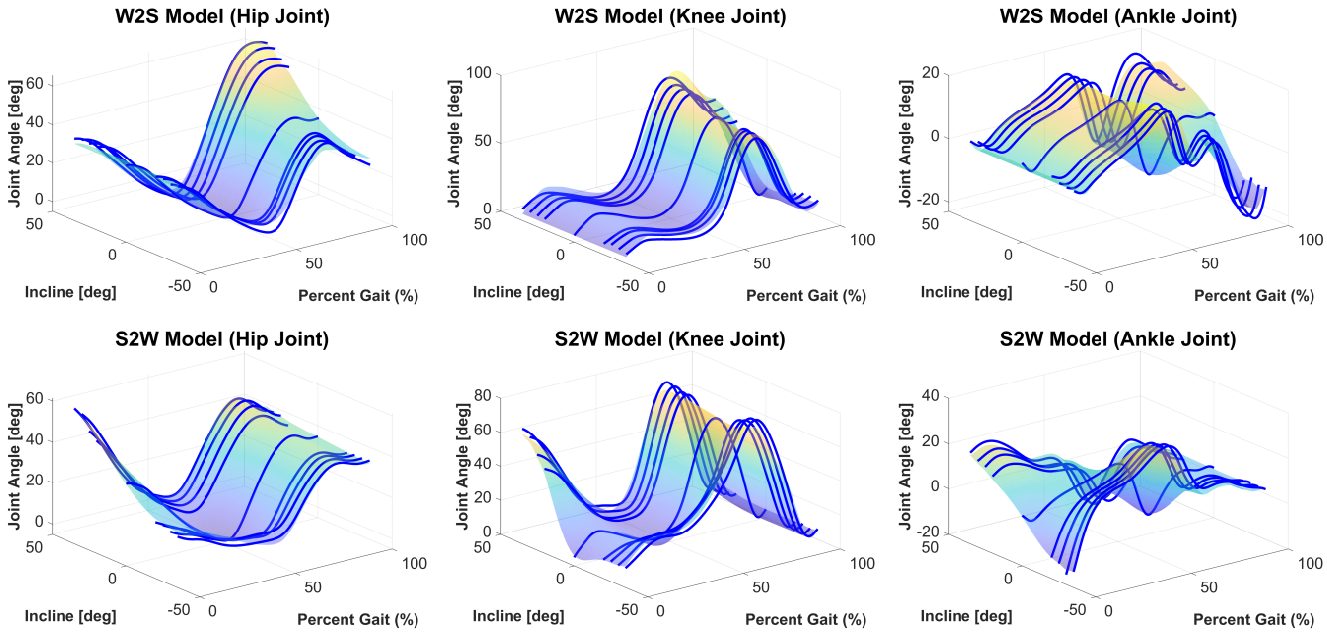

Fig. 3. Final continuously-varying W2S (top) and S2W (bottom) model for the hip, knee, and ankle joint generated using all the training data (blue lines). Level walking data was included to enable the extrapolation of transition walking trajectories at lower inclinations (i.e., lower than 20°).

between walking and walk to stair transitions, so we also study how such errors will affect the predicted joint kinematics at different ground inclinations ($-10°$ to $10°$). We compare the simulated output results from the W2S model with the SSW model at the same inclinations based on the RMSEs normalized with the range of motion (ROM) for each joint.

III. RESULTS

We now summarize the cross-validation results for the steady-state and transition models and present the final models and associated errors when trained with all available data in the dataset [25]. Next, we show the simulation results to evaluate the robustness of the models against incline input perturbations and ambulation mode misclassification during walking. Note that the SSW model is based on the same methods in [9] but evaluated with a different multi-activity dataset.

A. Model Performance

Table I contains the leave-one-inclination-out validation results for each model, while Table II summarizes the final model errors evaluated with all the training data to show how the proposed modeling framework fits the complete training dataset. The maximum (over all joints and all models) of the mean RMSE value was 3.59° and 3.05° for the cross-validation and final model errors, respectively. Both of the maximum RMSE values occur at the knee joint in the W2S model. Over all the models, the knee joint tended to have higher errors than the other two joints. The W2S model had the worst mean RMSE over all joints in the final model. The final continuously-varying kinematic surfaces of the hip, knee, and ankle joints trained (using all the available training data) for the steady-state and transition models are shown in Fig. 2 and Fig. 3, respectively.

The mean training times for the SSW model were 6.62 s for the hip, 6.68 s for the knee, and 6.76 s for the ankle. For the SSS model, the mean training times were 7.89 s, 9.75 s, and 6.44 s for the hip, knee, and ankle, respectively. Finally for the transition models, including both W2S and S2W, the mean training time was 0.84 ms for the hip, 0.82 ms for the knee, and 0.83 ms for the ankle. These quick training times illustrate one advantage of the convex modeling framework, requiring at most a few seconds to generate the entire model.

The resulting models only involve matrix multiplication and addition to output joint angles given required inputs, so the

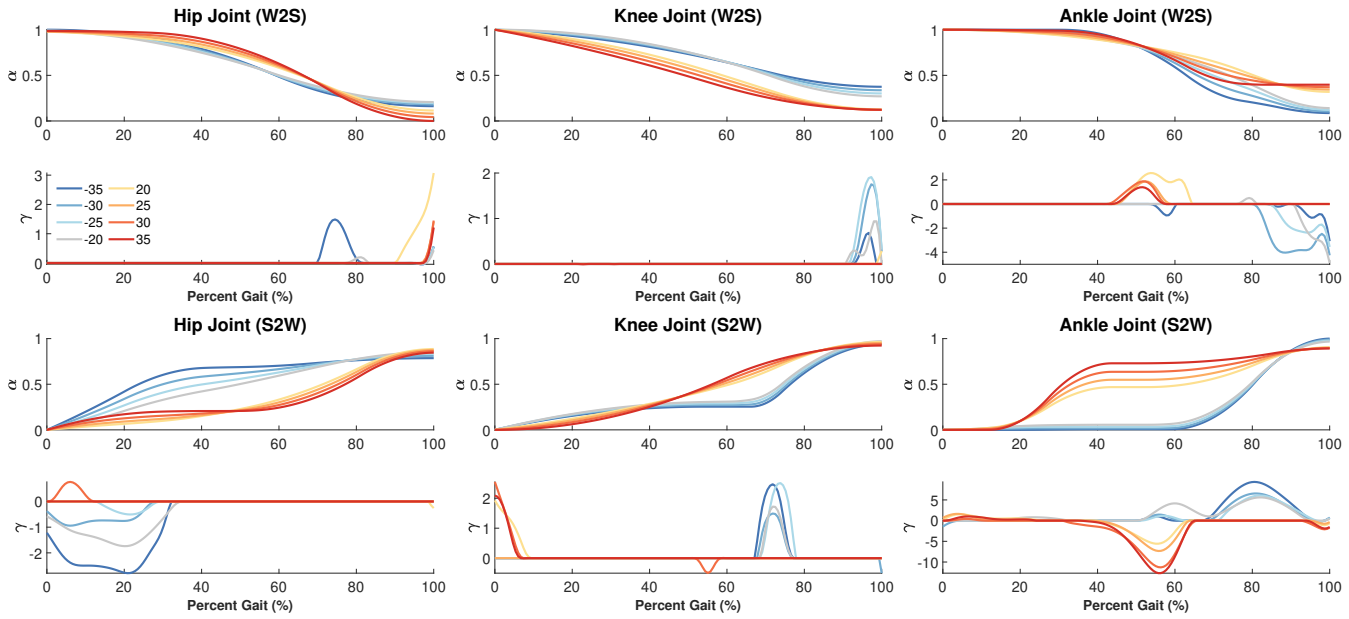

Fig. 4. Visualization of the interpolation coefficients for the W2S model. α equals 1 and 0 when the transition trajectory is close to the steady-state walk and stair trajectory, respectively. The offset term γ applies only when the transition trajectory is outside the convex hull created by those two steady-state models. Lines in cold colors (e.g., grey and blue) represent the negative stair inclines (stair descent), whereas the lines in warm colors (e.g., yellow and red) represent the positive stair inclines (stair ascent). The units of the stair incline legend are in degrees.

average computation time was 0.011 ms, 0.012 ms, 0.043 ms, and 0.043 ms for the SSW, SSS, W2S, and S2W models, respectively. These times demonstrate the feasibility of real-time computation for future control applications.

B. Interpolation Coefficients of Transition Models

Fig. 4 shows the profiles of the interpolation coefficients used to formulate the transition models at different inclinations over phase. The coefficients of the convex combination (α) are plotted above the conditional offset (γ) for each joint of the W2S and S2W models. The coefficient α demonstrates the (nonlinear) progression from one steady-state model to the other, which can be interpreted as the transition variable describing how close the transition kinematics are to each steady-state model. A clear separation can be seen between the transition rates for stair ascent vs. stair descent in both W2S and S2W. While most of the conditional offsets (γ) appear towards the end of the gait cycle for the W2S model, they tend to occur at the beginning of the S2W model. The ankle joint for the S2W model is a special case with significant γ (in both duration and magnitude).

C. Model Robustness Simulation Results

The mean normalized RMSE (RMSE/ROM) of the steady-state and transition models converged after 12,000 Monte Carlo iterations with perturbed incline inputs. The SSW model yields a maximum RMSE/ROM of 5.97% for the hip joint, 6.78% for the knee joint, and 8.04% for the ankle joint, while the SSS model yields 7.35%, 5.26%, and 6.25% for the hip, knee, and ankle joints, respectively. The W2S model has a maximum RMSE/ROM of 2.99%, 3.88%, and 2.50% for the hip, knee, and ankle joints, respectively. The S2W model demonstrates a similar error for the hip (3.07%) and knee (4.02%) joints compared to the W2S model, but shows a higher error for the ankle (4.46%) joint. Example plots for the worst-case results during the simulations for the transition models are shown in Fig. 5. Supplementary Table S2 summarizes the inclines (nominal and perturbed) where the worst cases are found over all the models and joints.

Considering ambulation mode misclassification, the normalized RMSEs (RMSE/ROM) between the SSW output and the output of W2S are shown in Fig. 6. The normalized RMSEs increase with the inclination for all the joints with a maximum error of 19.43%, 18.93%, and 27.32% and minimum error of 2.75%, 3.25%, and 4.41% for the hip, knee, and ankle joints, respectively.

IV. Discussion

A. Fitting Performance

In Section II-D2, we evaluated the ability of our models to interpolate untrained trajectories within the bounds of known inclinations. The results in Table I demonstrate the high model fitting performance for all the models with mean RMSEs of 2.04 $\pm$ 0.74°, 2.95 $\pm$ 1.44°, and 1.87 $\pm$ 0.59° for the hip, knee, and ankle during cross-validation. The other model errors (i.e., N_μ and N_m) are normalized by the inter-subject standard deviation of the experimental data. Therefore, they give a direct comparison between modeling error and subject variations. From Table I, the mean normalized error (N_μ) is always within half of the subject variation ($N_\mu < 0.5$), while the maximum normalized error (N_m) is always within the subject variation, except for the ankle joint of SSW model. The final maximum (over all joints) of the mean RMSEs for the knee (3.05°) and ankle (1.72°) of all the models are less

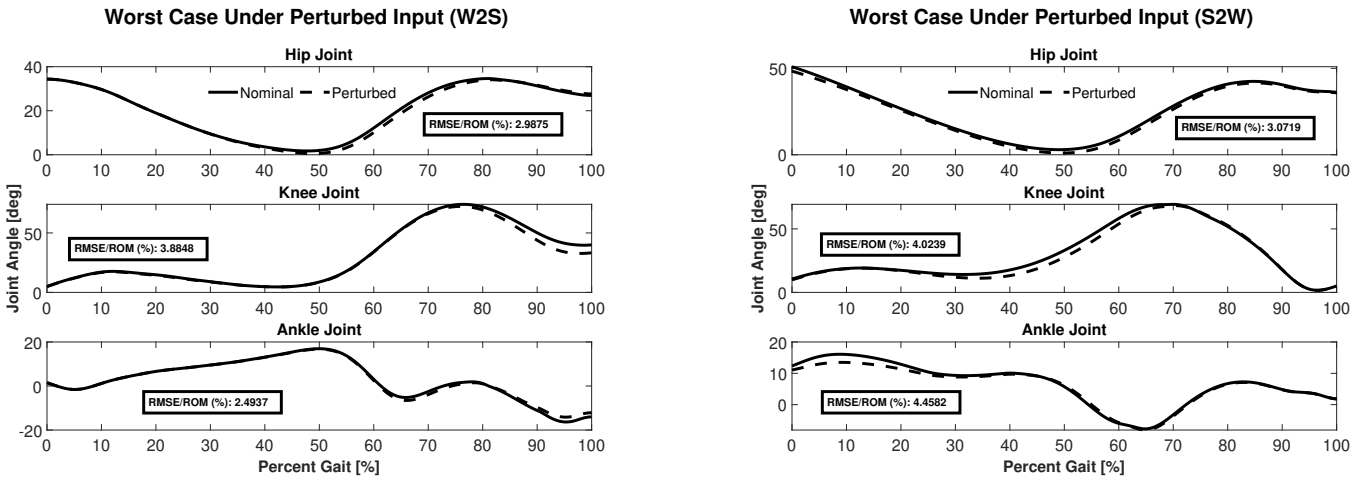

Fig. 5. Kinematic deviations for the worst-case scenario with perturbed incline input for the W2S and S2W joint models. For all the joints, the worst case occurs at the maximum simulated input error. Black solid lines indicate the nominal trajectories while the dashed lines represent the perturbed trajectories.

than the mean joint angle change that humans can perceive (knee $\approx 3.56°$ [33], ankle $\approx 2.33°$ [34]). Hence, we conclude that the proposed modeling framework can adequately fit the training data. Note that the cross-validation errors for SSW are higher than SSS mainly because the available training data (Section II-D1) for the SSW model comprises a sparser set of inclinations. In addition, our SSW model has similar fitting performance as the walking model generated with a different dataset in [9], which indicates the proposed modeling framework has a degree of invariance to the training dataset.

B. Interpretation of Interpolation Coefficients

One of the advantages of modeling transitions based on the associated steady-state models is to visualize how the transition occurs from the biomechanical perspective. In Fig. 4, the α coefficients describe how the joint kinematics transition from walk or stairs at each phase when there is no conditional offset. For example, we observed that some of the α trajectories indicate a relatively binary switch from one steady-state to the other (e.g., negative inclines for S2W at knee joint) while other trajectories demonstrate a more linear transition (e.g., positive inclines for S2W at knee joint).

For the walk to stair transition, the transition trajectory is close to walking first and tends to be more similar to stairs as the phase increases. Ideally, we expect α to end at 0, which indicates the transition is completed and the next stride will enter stair mode. However, for all joints and most of the inclines, α does not reach 0 at the end of the transition, especially for the hip and knee joints at negative inclines and the ankle joint at positive inclines. Even for those positive inclines that end close to 0 for the hip joint, e.g., 35°, the conditional offset is positive, which means the transition joint position at that point is higher than both walk and stair joint positions. One possible reason is that the transition is not completed within the first transition stride we analyzed, i.e., the subjects do not enter the steady-state stair mode with a one-stride transition. In fact, the subjects may not enter steady-state after the first two or even three steps based on the streaming data for the transition cycle in [25], as the trajectories in these strides are not fully periodic. However, these trajectories are close enough to periodic to facilitate stair ascent with a periodic model as seen in [35]. Increasing the number of transition strides in our transition models may facilitate even smoother transitions. In addition, we observe some conditional offsets during mid-swing for the hip joint at negative inclines and during push-off for the ankle joint at both positive and negative inclinations, indicating potentially exaggerated motion during the transition. For example, the subject could over- or under-estimate the pushoff required to rise the stairs during the transition stride. Finally, some transition trajectories leave the convex hull between steady-state trajectories at certain gait events due to phase shifts (e.g., maximum hip flexion for W2S at $-35°$ occurs between the corresponding phases of the walk and stair cases).

In contrast with the walk to stair transition, the stair to walk transition tends to have a conditional offset at the beginning of the stride for the hip and knee joints, while the offsets are more significant for the ankle joint in terms of both magnitude and duration. The conditional offset applies if and only if the transition trajectory is outside the convex hull created by the walk and stair trajectories, suggesting the transition joint angle at those early phases is out of the bound. One possible reason is that the subject may leave the steady-state gait before the transition occurs in order to prepare for the transition, which results in different kinematics during the pre-transition step [22]. The knee joint has some conditional offsets during mid-swing due to the shift in gait phase at maximum knee flexion. Finally, the ankle joint is the worst-case since the transition trajectories are outside the convex hull of the walk and stair trajectories at many phases and inclinations. An extreme case occurs at the singularity point in Fig. 1(b), where the walk and stair trajectories intersect at 0° while the transition joint angle has a higher value. In this situation, the model cannot fit the transition trajectory without an offset. However, most of the α trajectories tend to end at 1, and there are only a few small conditional offsets at the end of the gait cycle for the S2W

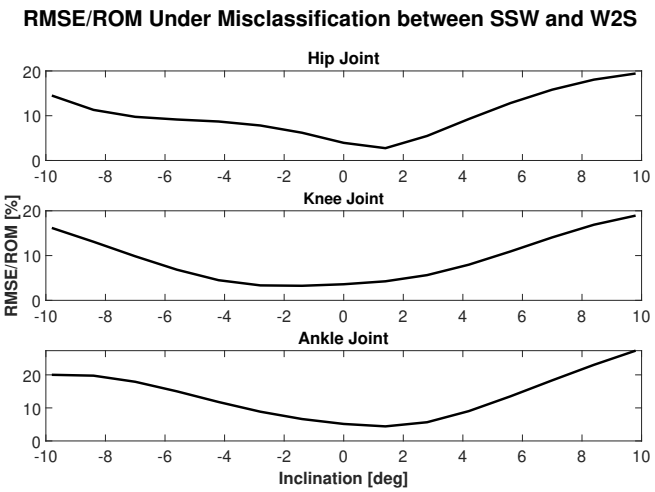

Fig. 6. Misclassification results during walking at different inclinations. The black lines refer to the RMSE values between the kinematics predicted for the SSW and W2S trajectories at the same inclination over the entire stride. All RMSE values were normalized by the range of motion (ROM) of the joint.

model. This means the transition joint angle matches with the walk model very well and it is possible to finish the transition with one stride for this case.

Another possible reason for non-zero conditional offsets at the extremes of the gait cycle is gait segmentation errors from the experiment data processing in [25]. In this dataset, although walking was segmented automatically based on the treadmill force plates, the stair trials required manual segmentation based on heel markers, introducing more uncertainty. According to Fig. 4, the offsets occur frequently towards the end of the gait cycle for W2S and at the beginning of the gait cycle for S2W, showing that offsets are more likely to occur on the stairs compared to the ground. Post-processing analysis shows that time-shifting the x-axis by 8 ms can result in joint angle changes of approximately 2 degrees at the ankle joint in certain tasks. Those joint angle differences are compatible with the magnitude of the offsets at the extremes of the gait cycle in Fig. 4, which demonstrates that small segmentation errors can possibly contribute to the offsets at heel strikes. However, this would not explain the offset in the middle of the gait cycle, such as in Fig. 1(b).

C. Integration with Robotic Prosthesis Controllers

The presented models provide the basis for a position-based prosthetic leg controller that continuously spans ambulation modes (walk vs. stairs) and their task conditions (i.e., speed, inclines). The transition models are trained based on the steady-state models to parameterize the continuum between steady-state ambulation modes according to the interpolation coefficient α, which we call a *transition variable*. This transition variable equals zero for stairs, one for walk, or an intermediate value corresponding to the progression of a transition between modes. A finite state machine using activity/intent recognition methods (e.g., [32], [36]) can determine which model to employ and when to begin calculating a transition variable. Once a transition stride has been detected, the transition variable can be determined by a phase variable (in place of percent gait) and the monotonic relationships established in Fig. 4. The task condition inputs can be determined using speed/incline detection methods. We next discuss the practicality of task variable estimation and activity mode classification for future implementations and the potential consequences for individuals with lower-limb amputation.

1) Task Condition Measurement and Prediction: State-of-the-art methods can measure the forward speed and inclination/height for ramp and stair ambulation in real-time [20], [31] in order to provide task condition inputs to the steady-state models (and thus the transition models). However, to begin a stride with the correct trajectories, it is desirable to have all the input information by the start of the stride. A Deep Convolutional Neural Network and 2D point cloud [37] can obtain the ramp inclination or stair height before each stride (including transitions). Although the speed estimators in [20], [31] focused on the walking case, those methods can be theoretically extended to the stair case. These speed and incline estimators can enable the steady-state and transition models to predict appropriate joint kinematics in real-time to ensure seamless multi-activity locomotion.

In addition, the simulation under perturbed input from Section III demonstrates the robustness of the models against input estimation errors. The maximum normalized RMSE with respect to the range of motion for the steady-state models is 8.04%, which occurs at the ankle joint of SSW. The normalized RMSEs for SSW are high mainly because the range of perturbations is large relative to the range of possible inclines. During the simulation on the SSS model, we observed a phase shift for the perturbed trajectory compared to the nominal trajectory for inclines around $\pm 20°$, which caused higher normalized RMSEs compared to the other simulated inclinations. This is likely because the timings of gait events (e.g., maximum hip flexion) start to resemble walking as inclines decrease below 20° (recall that level walking kinematics were used to connect stair ascent and stair descent in SSS). However, gait events are fairly consistent in SSW because of the similarity in kinematics between level walking and inclined walking. Therefore, we did not observe phase shifts in SSW during these simulations.

The transition models are even more robust under input perturbation than the steady-state models, noting the lower maximum normalized RMSEs for both transition models in Fig. 5. The additional jerk minimization on the interpolation coefficients further smoothed the continuously-varying surfaces in Fig. 3. The maximum normalized RMSE over all conditions is 4.46% at the ankle joint for the stair to walk transition. The transition models can still generate reasonably accurate trajectories at the boundary of the incline error range (i.e., 3.0°). Therefore, even if we do not have the stair inclination before the transition, we can assume a nominal stair incline as the initial input and correct that during $60\% - 80\%$ of the transition stride using the correlation between hip range of motion and the stair inclination. Because our models are continuously-varying across inputs, we could still generate the continuous kinematics trajectories by linearly varying the input from the nominal to the actual value during the transition.

2) Ambulation Mode Classification: Machine learning or deep learning algorithms have shown promising results in intent recognition. Some existing methods predict the transition before it happens [22], [23], [37], which could be used to implement the transition model and initiate calculation of the transition variable at the beginning of the transition stride.

Moreover, Fig. 6 demonstrates the robustness of the model against the misclassification. That is, if the ambulation mode is incorrectly estimated during walking (e.g., falsely switches to W2S), the resulting kinematic trajectory will be similar to the correct trajectory at low inclinations. Although the difference between trajectories generated by these two models is more significant at higher inclinations (maximum normalized RMSE of 27.32%), it is also more likely to have an accurate estimation of the ambulation mode using the transition prediction methods mentioned above due to the larger difference between the kinematics of steady states and transitions.

3) Implications for Amputee Subjects: The main objective of using able-bodied data to train the kinematic model for prosthesis control is to emulate able-bodied leg biomechanics, which in turn may help restore physiological gait in individuals with lower-limb amputation. Our prior and recent studies have shown that able-bodied references for controlling powered prosthetic legs can enable above-knee amputee users to walk in a more normative manner over variable inclines [5], [20], [38]. Preliminary results with an able-bodied bypass user indicate similar potential for stair ascent [35]. Therefore, the kinematic models generated by the presented framework could yield similarly promising results over a continuum of walking and stair climbing activities, including both steady-state and transitional gaits.

D. Limitations and Future Work

The proposed modeling framework has several limitations. First, it requires at least some labeled data at different task conditions and at the extremes of the task condition space to generate the continuously-varying models. Since the stair and transition data are unlabeled for speed in the training dataset used in this paper, we could not predict the trend of speed change for those models. Second, the able-bodied data used to generate the models may not account for anatomical changes due to limb amputation (e.g., muscle atrophy) that contribute to permanently altered gait biomechanics. Thirdly, the model would likely perform better for specific users if it was trained using individualized kinematic data [39], as we assumed average instead of subject-specific kinematics during model training. However, the presented framework can be used to quickly retrain the models within a few seconds (Section III-A) during clinical sessions for tuning the reference kinematics for high-priority activities [40].

Future work includes the real-time implementation of the activity mode classifiers and task condition estimators needed to use the presented models, and the experimental validation of the unified position-based controller on a powered prosthetic leg (e.g., [3]). These implementations could include environment feature inputs such as the distance from obstacles or stairs (with LiDar or depth camera) to enable timely transitions. Joint kinetics could also be considered by expanding the suggested framework to model continuously-varying impedance parameters, as exemplified by the walking controller in [38]. Such an impedance framework would account for physical interaction with the environment in a more compliant and biomimetic manner.

V. CONCLUSIONS

This paper presents a modeling framework based on averaged able-bodied kinematics to generate steady-state and transition models. Both the steady-state models (SSS, SSW) parameterize human locomotion as a function of gait phase, forward speed, and inclines, while both the transition models (W2S, S2W) are set up as a convex combination of those two steady-state models with a conditional offset. The cross-validation results illustrate that all models have the ability to accurately interpolate untrained trajectories, and the simulation results demonstrate the robustness of the models against perturbed input and ambulation model misclassification. The interpolation coefficients visualize the connection between transitional kinematics and steady-state kinematics and demonstrate biomechanical meaning behind the transitions. These models will also enable a new continuously-varying paradigm for position-based control of powered prosthetic legs over different task conditions and ambulation modes, which can be adapted for impedance control in future work.

ACKNOWLEDGMENT

The authors thank Kevin Best, Emma Reznick, and Ross Cortino for meaningful discussion, and Kyle Embry for sharing source code for the continuously-varying walking model. The authors also thank Yuye Zhang for contributing to the design of the graphical abstract.

REFERENCES

[1] F. Sup, H. A. Varol, and M. Goldfarb, "Upslope walking with a powered knee and ankle prosthesis: Initial results with an amputee subject," *IEEE Trans. Neural Syst. Rehabil. Eng.*, vol. 19, no. 1, pp. 71–78, 2011.

[2] B. E. Lawson, H. A. Varol, A. Huff, E. Erdemir, and M. Goldfarb, "Control of stair ascent and descent with a powered transfemoral prosthesis," *IEEE Trans. Neural Syst. Rehabil. Eng.*, vol. 21, no. 3, pp. 466–473, 2013.

[3] T. Elery, S. Rezazadeh, C. Nesler, and R. D. Gregg, "Design and validation of a powered knee–ankle prosthesis with high-torque, low-impedance actuators," *IEEE Transactions on Robotics*, vol. 36, no. 6, pp. 1649–1668, 2020.

[4] C. Jayaraman, S. Hoppe-Ludwig, S. Deems-Dluhy, M. McGuire, C. Mummidisetty, R. Siegal, A. Naef, B. E. Lawson, M. Goldfarb, K. E. Gordon *et al.*, "Impact of powered knee-ankle prosthesis on low back muscle mechanics in transfemoral amputees: A case series," *Frontiers in neuroscience*, vol. 12, p. 134, 2018.

[5] D. Quintero, D. Villarreal, D. Lambert, S. Kapp, and R. Gregg, "Continuous-phase control of a powered knee-ankle prosthesis: Amputee experiments across speeds and inclines," *IEEE Trans. Robot.*, vol. 34, no. 3, pp. 686–701, 2018.

[6] S. Rezazadeh, D. Quintero, N. Divekar, E. Reznick, L. Gray, and R. D. Gregg, "A phase variable approach for improved rhythmic and non-rhythmic control of a powered knee-ankle prosthesis," *IEEE Access*, vol. 7, pp. 109 840–109 855, 2019.

[7] M. A. Holgate, T. G. Sugar, and A. W. Bohler, "A novel control algorithm for wearable robotics using phase plane invariants," in *2009 IEEE Int. Conf. Robotics and Automation*, 2009, pp. 3845–3850.

[8] N. Dhir, H. Dallali, E. M. Ficanha, G. A. Ribeiro, and M. Rastgaar, "Locomotion envelopes for adaptive control of powered ankle prostheses," in *Proc. IEEE Int. Conf. Robot. Autom.*, 2018, pp. 1488–1495.

[9] K. R. Embry, D. J. Villarreal, R. L. Macaluso, and R. D. Gregg, "Modeling the kinematics of human locomotion over continuously varying speeds and inclines," *IEEE Trans. Neural Syst. Rehabil. Eng.*, vol. 26, no. 12, pp. 2342–2350, 2018.

[10] K. R. Embry and R. D. Gregg, "Analysis of continuously varying kinematics for prosthetic leg control applications," *IEEE Trans. Neural Syst. Rehabil. Eng.*, vol. 29, pp. 262–272, 2021.

[11] J. Zhu, Q. Wang, and L. Wang, "On the design of a powered transtibial prosthesis with stiffness adaptable ankle and toe joints," *IEEE Transactions on Industrial Electronics*, vol. 61, no. 9, pp. 4797–4807, 2014.

[12] B. E. Lawson, J. Mitchell, D. Truex, A. Shultz, E. Ledoux, and M. Goldfarb, "A robotic leg prosthesis: Design, control, and implementation," *IEEE Robotics Automation Magazine*, vol. 21, no. 4, pp. 70–81, 2014.

[13] A. M. Simon, K. A. Ingraham, J. A. Spanias, A. J. Young, S. B. Finucane, E. G. Halsne, and L. J. Hargrove, "Delaying ambulation mode transition decisions improves accuracy of a flexible control system for powered knee-ankle prosthesis," *IEEE Trans. Neural Syst. Rehabil. Eng.*, vol. 25, no. 8, pp. 1164–1171, 2017.

[14] H. L. Bartlett and M. Goldfarb, "A phase variable approach for imu-based locomotion activity recognition," *IEEE Trans. Biomed. Eng.*, vol. 65, no. 6, pp. 1330–1338, 2018.

[15] S. Gao, J. Mai, J. Zhu, and Q. Wang, "Mechanism and controller design of a transfemoral prosthesis with electrohydraulic knee and motor-driven ankle," *IEEE/ASME Transactions on Mechatronics*, vol. 26, no. 5, pp. 2429–2439, 2021.

[16] M. Tucker, J. Olivier, A. Pagel, H. Bleuler, M. Bouri, O. Lambercy, J. del Millán, R. Riener, H. Vallery, and R. Gassert, "Control strategies for active lower extremity prosthetics and orthotics: A review," *J. NeuroEngineering and Rehabilitation*, vol. 12, no. 1, pp. 1–29, 2015.

[17] M. F. Eilenberg, H. Geyer, and H. Herr, "Control of a powered ankle–foot prosthesis based on a neuromuscular model," *IEEE Trans. Neural Syst. Rehabil. Eng.*, vol. 18, no. 2, pp. 164–173, 2010.

[18] A. Simon, K. Ingraham, N. Fey, S. Finucane, R. Lipschutz, A. Young, and L. Hargrove, "Configuring a powered knee and ankle prosthesis for transfemoral amputees within five specific ambulation modes," *PloS one*, vol. 9, p. e99387, 06 2014.

[19] C. E. Roffman, J. Buchanan, and G. T. Allison, "Predictors of non-use of prostheses by people with lower limb amputation after discharge from rehabilitation: development and validation of clinical prediction rules," *J. Physiotherapy*, vol. 60, no. 4, pp. 224–231, 2014.

[20] K. Best, K. Embry, E. Rouse, and R. Gregg, "Phase-variable control of a powered knee-ankle prosthesis over continuously varying speeds and inclines," in *IEEE Int. Conf. Intelligent Robots & Systems*, 2021.

[21] F. Zhang, M. Liu, and H. Huang, "Investigation of timing to switch control mode in powered knee prostheses during task transitions," *PloS one*, vol. 10, p. e0133965, 2015.

[22] J. Figueiredo, S. P. Carvalho, D. Gonçalve, J. C. Moreno, and C. P. Santos, "Daily locomotion recognition and prediction: A kinematic data-based machine learning approach," *IEEE Access*, vol. 8, 2020.

[23] K. Zhang, J. Luo, C. Fu, W. Xiao, W. Zhang, H. Liu, J. Zhu, Z. Lu, Y. Rong, and C. Silva, "A subvision system for enhancing the environmental adaptability of the powered transfemoral prosthesis," *IEEE Transactions on Cybernetics*, vol. PP, pp. 1–13, 03 2020.

[24] J. Peng, N. P. Fey, T. A. Kuiken, and L. J. Hargrove, "Anticipatory kinematics and muscle activity preceding transitions from level-ground walking to stair ascent and descent," *Journal of Biomechanics*, vol. 49, pp. 528–536, 2 2016.

[25] E. Reznick, K. Embry, R. Neuman, E. Bolívar-Nieto, N. Fey, and R. Gregg, "Lower-limb kinematics and kinetics during continuously varying human locomotion," *Scientific Data*, vol. 8, 10 2021.

[26] S. Boyd and L. Vandenberghe, *Convex optimization*. Cambridge university press, 2004.

[27] B. Cyganek, *Object Detection and Recognition in Digital Images*. John Wiley & Sons Ltd, 6 2013.

[28] T. Lenzi, L. Hargrove, and J. Sensinger, "Speed-adaptation mechanism: Robotic prostheses can actively regulate joint torque," *IEEE Robotics Automation Magazine*, vol. 21, no. 4, pp. 94–107, 2014.

[29] F. Leboeuf, R. Baker, A. Barré, J. Reay, R. Jones, and M. Sangeux, "The conventional gait model, an open-source implementation that reproduces the past but prepares for the future," *Gait and Posture*, vol. 69, pp. 126–129, mar 2019.

[30] J. Lee, W. Hong, and P. Hur, "Continuous gait phase estimation using lstm for robotic transfemoral prosthesis across walking speeds," *IEEE Trans. Neural Syst. Rehabil. Eng.*, vol. 29, pp. 1470–1477, 2021.

[31] J. Camargo, W. Flanagan, N. Csomay-Shanklin, B. Kanwar, and A. Young, "A machine learning strategy for locomotion classification and parameter estimation using fusion of wearable sensors," *IEEE Trans. Biomed. Eng.*, vol. 68, no. 5, pp. 1569–1578, 2021.

[32] S. Cheng, E. Bolívar-Nieto, and R. D. Gregg, "Real-time activity recognition with instantaneous characteristic features of thigh kinematics," *IEEE Trans. Neural Syst. Rehabil. Eng.*, vol. 29, pp. 1827–1837, 2021.

[33] D. Barrett, A. Cobb, and G. Bentley, "Joint proprioception in normal osteoarthritic and replaced knees," *The Journal of bone and joint surgery. British volume*, vol. 73, pp. 53–6, 02 1991.

[34] N. Deshpande, D. M. Connelly, E. G. Culham, and P. A. Costigan, "Reliability and validity of ankle proprioceptive measures," *Archives of Physical Medicine and Rehabilitation*, vol. 84, pp. 883–889, 6 2003.

[35] R. Cortino, E. Bolívar-Nieto, K. Best, and R. Gregg, "Stair ascent phase-variable control of a powered knee-ankle prosthesis," in *IEEE Int. Conf. Robotics & Automation*, 2022.

[36] B. Hu, A. M. Simon, and L. Hargrove, "Deep generative models with data augmentation to learn robust representations of movement intention for powered leg prostheses," *IEEE Transactions on Medical Robotics and Bionics*, vol. 1, no. 4, pp. 267–278, 2019.

[37] K. Zhang, C. Xiong, W. Zhang, H. Liu, D. Lai, Y. Rong, and C. Fu, "Environmental features recognition for lower limb prostheses toward predictive walking," *IEEE Trans. Neural Syst. Rehabil. Eng.*, vol. PP, pp. 1–1, 01 2019.

[38] T. Best, C. Welker, E. Rouse, and R. Gregg, "Phase-based impedance control of a powered knee-ankle prosthesis for tuning-free locomotion over speeds and inclines," 2022. [Online]. Available: https://www.techrxiv.org/articles/preprint/Phase-Based_Impedance_Control_of_a_Powered_Knee-Ankle_Prosthesis_for_Tuning-Free_Locomotion_over_Speeds_and_Inclines/19165895/1

[39] E. Reznick, K. Embry, and R. D. Gregg, "Predicting individualized joint kinematics over a continuous range of slopes and speeds," in *Proc. 8th IEEE RAS/EMBS Int. Conf. Biomed. Robot. Biomechtron. (BioRob)*, 2020, pp. 666–672.

[40] D. Quintero, E. Reznick, D. J. Lambert, S. Rezazadeh, L. Gray, and R. D. Gregg, "Intuitive clinician control interface for a powered knee-ankle prosthesis: A case study," *IEEE journal of translational engineering in health and medicine*, vol. 6, pp. 1–9, 2018.